Applied Physics A (2026) 132:326
https://doi.org/10.1007/s00339-026-09515-0

Applied Physics A
Materials Science & Processing

Effects of flame spray coating of Al_2O_3–TiO_2 on the structural and mechanical properties of boron steel surfaces

Gozde Altuntas[1] · Fatih Altun[2] · Abdülcelil Bayar[3,4] · Ramazan Asmatulu[2] · Bülent Bostan[1]

Received: 27 August 2025 / Accepted: 8 March 2026
© The Author(s) 2026

Abstract

In this study, a boron-alloyed microalloyed steel was subjected to austenitizing and tempering heat treatments, followed by surface coating using the flame spray technique. Ceramic powders containing 87% Al_2O_3 and 13% TiO_2 with an average particle size of approximately 50 μm were used to produce coatings at three different thicknesses. Prior to coating, surface preparation was performed by sandblasting treatment to ensure optimal adhesion. After the coating process, the density of the coatings was measured using the Archimedes principle to indirectly assess porosity, interfacial bonding quality, and overall coating integrity. The phase structure, crystallinity, and structural transformations of the coated surfaces were analyzed by X-ray diffraction (XRD). Additionally, dislocation density values were calculated from the XRD data to evaluate the crystallographic characteristics of the coatings. The mechanical performance was assessed through wear tests and hardness measurements conducted on both coated and uncoated samples. The results demonstrated that the flame spray coating significantly enhanced the surface properties of the boron-alloyed steel, providing up to a 45% improvement in wear resistance. Furthermore, salt spray corrosion testing revealed that the coated specimens exhibited superior corrosion resistance without any visible surface degradation, highlighting the effective environmental protection offered by the Al_2O_3–TiO_2 ceramic coating.

Keywords Flame Spray Coating · Boron-alloyed Steel · Crystallinity · Wear · Corrosion.

1 Introduction

Boron-alloyed microalloyed steel is a special type of steel obtained by adding very small amounts of boron (approximately 0.001–0.005 wt%) and typically microalloying elements (such as Ti, Nb, or V) to low-carbon steels. The boron content is kept at these low levels because higher amounts (e.g., above 0.01%) can cause embrittlement [1, 2]. This type of steel is widely used in the automotive and agricultural machinery sectors due to its high strength and hardenability. Although alternative lightweight materials such as aluminum and carbon fiber-reinforced composites are evaluated for their ability to reduce fuel consumption, they also significantly increase the overall cost of vehicles [3, 4]. Therefore, steel continues to play a vital role in automotive manufacturing, and steel producers are constantly working on developing new grades tailored for automotive applications. One of the main challenges associated with boron steels is their high strength, which can lead to difficulties during metal forming processes. The complex geometries of automotive components often result in increased springback during forming operations [5]. As a result, hot forming techniques are commonly used for these steels. However, hot forming introduces new challenges, such as oxidation, scale formation on the workpiece surface, and increased wear on forming dies. To mitigate scale formation and simultaneously improve corrosion and wear resistance, Al-Si coatings have been increasingly applied to the material surface [6, 7]. In several studies, aluminide coatings have been reported to form an alumina-rich surface layer, enhancing the high-temperature oxidation resistance of

✉ Gozde Altuntas
gozdealtuntas@gazi.edu.tr

[1] Department of Metallurgical and Materials Engineering, Gazi University, 06560 Ankara, Türkiye

[2] Department of Mechanical Engineering, Wichita State University, 1845 Fairmount Street, Wichita, KS 67260, USA

[3] Institute of Science, Gazi University, Ankara, Türkiye

[4] Department of Materials Engineering, Wichita State Unıversity, Wichita, USA

Published online: 26 March 2026

steels [8, 9]. For example, AlSi10Fe3-based coatings have been successfully applied to the surfaces of boron steels via hot-dip methods [10]. Nevertheless, conventional coating techniques often face limitations when applied to large or non-portable components. In contrast, the flame spray technique offers a practical advantage in such cases due to its portability and ease of on-site application. Moreover, its ability to coat only specific areas helps reduce material consumption [11–14]. Additionally, boron steels can be further strengthened through optimized heat treatment cycles, leading to martensitic or bainitic microstructures [15]. El-Shennawy et al. studied the mechanical properties of boron steels austenitized and quenched in different media [16]. Güler et al. investigated their mechanical and microstructural behavior under varying austenitizing temperatures and holding times [17]. Altuntaş et al. enhanced the mechanical performance of boron steels through tempering and cryogenic treatments, resulting in the development of advanced materials [18]. These studies demonstrate that proper heat treatments can significantly enhance the mechanical properties of boron steels, making them highly suitable for structural automotive components. As quenched and tempered steels, boron steels offer outstanding formability and high strength after heat treatment [19].

In the present study, hot-formed boron steel was subjected to a specific heat treatment and then coated using the flame spray method with ceramic powders composed of 87% Al_2O_3 and 13% TiO_2. Unlike previous studies in the literature, this work proposes an innovative approach by combining optimized heat treatment with thermal spray coating, significantly improving both the wear and corrosion resistance of the material.

2 Experiment

2.1 Materials

The boron microalloy steel used in the experimental studies was supplied hot-formed from Asil Çelik. This material is coded as the main material. Its chemical composition is given in Table 1. This material was used in our studies without further modifications.

2.2 Methods

The boron steel material was austenitized at 900 °C for 10 min, followed by quenching in water and subsequently tempered at 450 °C for 120 min. This specimen is referred to as "heat-treated" in this study. After completing the heat treatment process, sandblasting treatment was performed to achieve the necessary surface roughness prior to coating. The sandblasted specimen was then coated with a powder mixture of Al_2O_3 (87%) + TiO_2 (13%) having an average particle size of approximately 10–30 µm, applied in varying coating thicknesses. Larger particles require greater thermal input to melt completely; if insufficiently heated, they can create lamellar discontinuities and higher local porosity. The coating thickness was primarily controlled by adjusting three process variables: spray distance, powder feed rate, and the number of torch passes. The number of torch passes was varied systematically, where two pass typically contributed approximately 50 µm of coating buildup depending on the process conditions. The acetylene–oxygen mixture was adjusted to a slightly reducing flame using a ratio of $C_2H_2/O_2 \approx 1.2{:}1$, which helps minimize excessive oxidation of the Al_2O_3–TiO_2 particles during deposition. The distance between the coating torch and the base material is set as 20 cm. A visual representation of the sandblasting treatment and coating process is shown in Fig. 1.

The porosity levels of the coated samples were evaluated by measuring their densities using the Archimedes principle. To support these findings, microstructural examinations were also performed. After metallographic preparation of the cross-sections of the coated samples, the coating linearity, thickness, and adhesion quality were analyzed using a JEOL 6060LV Scanning Electron Microscope (SEM). Phase identification of.

both the coating and the substrate was carried out by X-ray diffraction (XRD) using a Bruker D8 Advance diffractometer. To assess the wear resistance of the coatings, data were obtained using a UTS brand wear testing machine. The wear experiments were carried out using a pin-on-disc tribometer under dry sliding conditions, while abrasion tests were performed at a distance of 1000 m at a load of 25 N. Additionally, to evaluate the corrosion resistance of the coating surface, microstructural surface inspections were performed after a 24-hour salt spray test.

3 Results and discussion

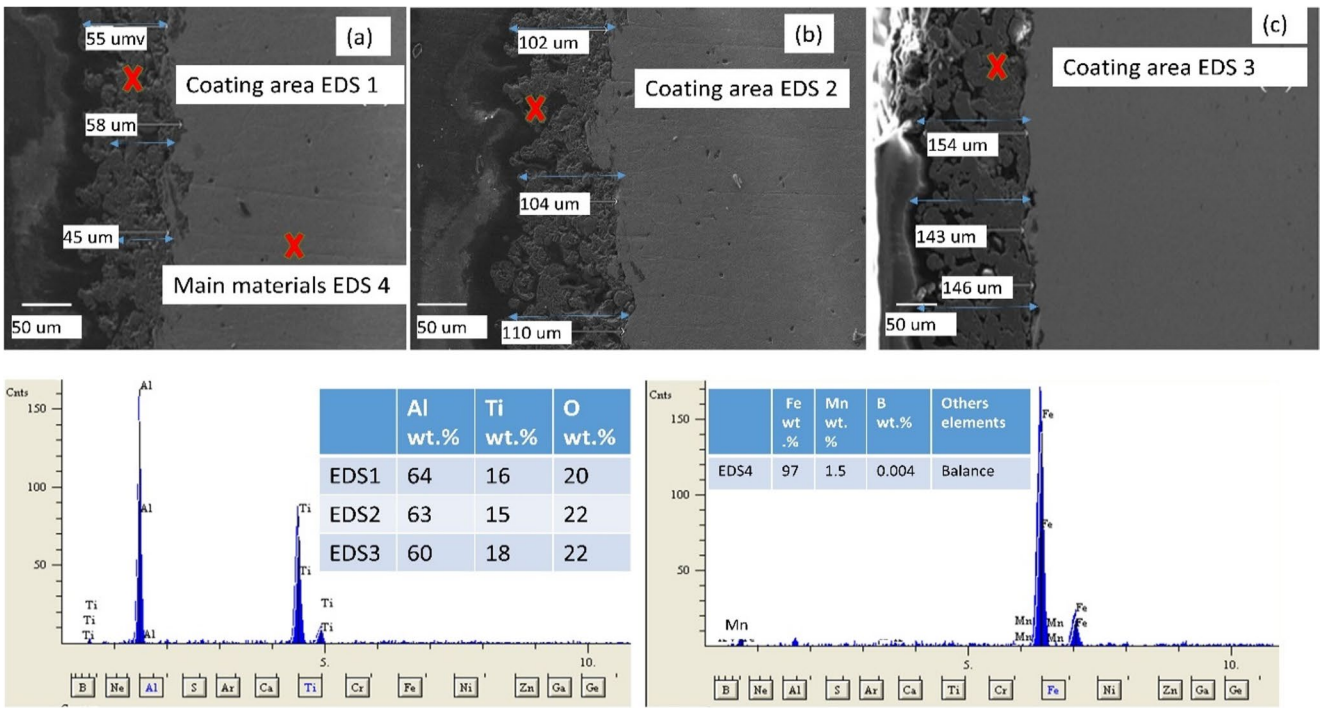
Figure 2 shows the SEM images of the cross-sections of the coated samples. SEM-EDS analysis was conducted to examine the homogeneity of the coating surface, porosity distribution, chemical composition, and coating thickness.

Table 1 Chemical composition of boron steel

Chemical Composition of Material (%)							
C	Si	Mn	P	S	Cr	Al	B
0.32	0.19	1.45	0.007	0.004	0.47	0.032	0.0033



Fig. 1 Visual of the sandblasting treatment process and coating stage



	Al wt.%	Ti wt.%	O wt.%
EDS1	64	16	20
EDS2	63	15	22
EDS3	60	18	22

	Fe wt .%	Mn wt. %	B wt.%	Others elements
EDS4	97	1.5	0.004	Balance

Fig. 2 Cross-sectional coating thickness measurements and EDS analyses of samples (**a**) 50 µm coating, (**b**) 100 µm coating, (**c**) 150 µm coating

It was observed that all coatings were well adhered to the substrate material. The density of a porous coating is expected to be lower than that of a fully dense coating made from the same material [20]. Therefore, the SEM micrographs also provided indirect information about the density of the coatings. The coating thicknesses were found to be consistent with the targeted average values, as observed in the microstructures. The porous morphology in the coating area is partly due to molten particles, rapid solidification, and lamellar voids specific to the flame spraying process. Optimization for this can be achieved with coating parameters. It was determined that approximately 50 µm coating thickness was achieved in 2 spray passes with the coating torch. To distinguish the chemical composition between the coating and the substrate, EDS analysis was performed, and the results revealed the elemental distribution across the interface. The measured regions (left part of the microstructure) represent the coating and the right part represents the parent material.

Microstructural examinations revealed the presence of voids formed during the coating process. This is an expected phenomenon in the flame spray coating technique [13]. Despite the presence and quantity of porosity, wear coefficient calculations were performed to determine how the mechanical properties were affected. For accurate wear coefficient determination, the density of each sample was measured using the Archimedes principle. The density of the base material and the heat-treated sample was

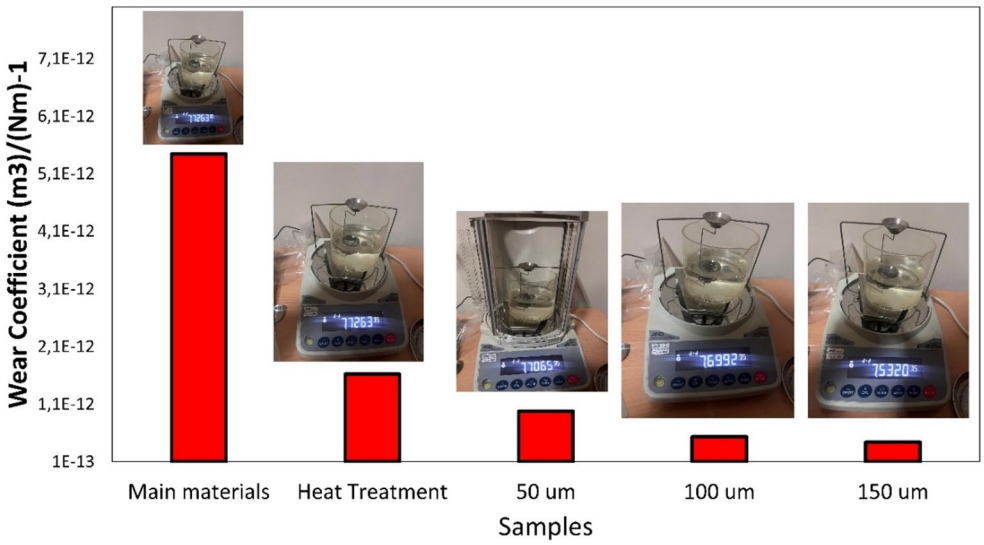


Fig. 3 Wear coefficient graphs and density measurements of samples

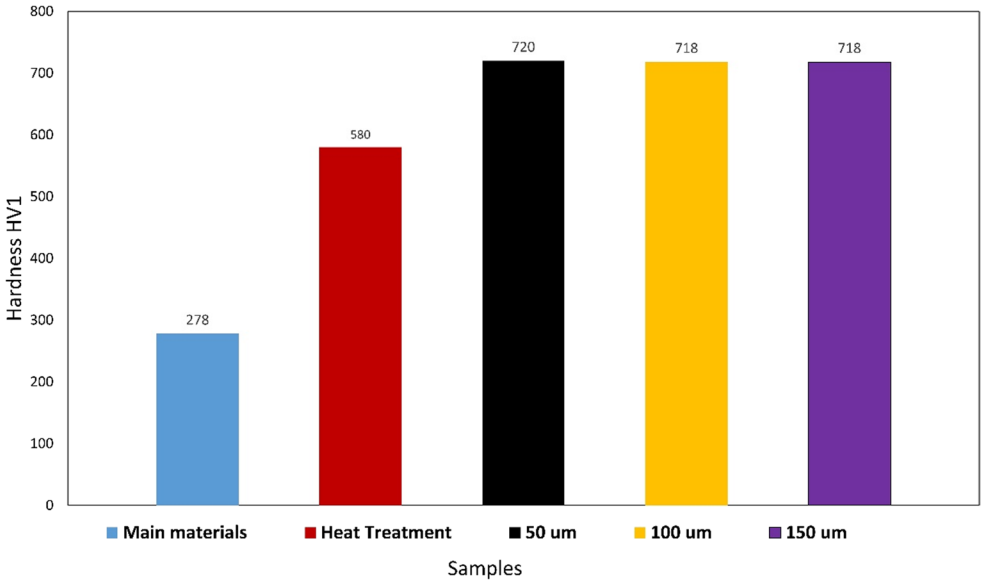


Fig. 4 Hardness measurement values of samples

measured as 7.72 g/cm^3, the 50 µm coated sample as 7.70 g/cm^3, the 100 µm coated sample as 7.69 g/cm^3, and the 150 µm coated sample as 7.53 g/cm^3. The density values show that the 150 µm coated sample has decreased significantly compared to the initial density, which may be associated with voids and other defects. These density values are also reflected in the wear coefficient graphs shown in Fig. 3. In general, coatings with varying thicknesses improved wear resistance. However, the coating thickness must be optimized, as excessive thickness can lead to the formation of cracks and increased porosity on the surface [21]. If the wear test is intended to evaluate the overall performance of the coated material (including both coating and substrate), the bulk density of the entire sample should be considered. This approach provides results that better reflect real-world service conditions, as the coating and the base material act together under load [22]. A higher wear coefficient indicates greater material loss, meaning lower wear resistance. The results showed that the uncoated material exhibited the highest wear coefficient. As the coating thickness increased, the overall density of the coated samples tended to decrease. This decrease was attributed to both the porosity introduced during the coating process and the inherently lower density of the ceramic-based coating powders compared to steel [21, 23]. Wear coefficient values were calculated using Archard's equation.

Figure 4 presents the macrohardness measurements of the samples. A significant increase in hardness was observed as a result of the applied heat treatments. This enhancement is attributed to the formation of tempered martensite microstructure [24–27]. The hardness values of the coated samples after heat treatment were consistent with those typically reported in the literature for ceramic-based coatings [28]. Due to the surface roughness of the coatings, all

samples were ground using 2500-mesh abrasive paper prior to hardness measurements to ensure measurement accuracy.

X-ray diffraction (XRD) analysis was conducted to identify the diffraction peaks corresponding to both the coating and the substrate material. Additionally, the formation of compounds between Al_2O_3 and TiO_2 within the coating was detected. As the coating thickness increased, the intensity of the Al_2O_3 and TiO_2 peaks also increased. Figure 5 shows the XRD patterns for coatings with different thicknesses: (a) 50 µm, (b) 100 µm, and (c) 150 µm. Figure 5(d) presents the XRD pattern of the boron-alloyed steel substrate. Figure 5 (e) is the xrd graph of the heat-treated material. Dislocation density is an indicator of lattice distortions and internal stresses within the crystal structure [29]. Using the XRD data, changes in microstructure and the level of internal stress after coating were evaluated by calculating dislocation densities. However, dislocation density values can only be directly compared within the same crystal structure. Therefore, the dislocation densities of the coated layers were compared only among each other, and not directly with the substrate. The full width at half maximum (FWHM) values were determined and used to calculate the dislocation densities based on the Williamson–Hall method, as shown in Eqs. (1–2) [30]. Flame-sprayed Al_2O_3–TiO_2 coatings cool very rapidly, and thicker coatings experience higher thermal gradients and stronger quenching stresses. This results in more microstrain, local lattice distortion, and inter-splat incompatibility, which produce higher peak broadening (β). Since the Williamson–Hall equation separates crystallite size and microstrain components, increased strain directly increases the calculated dislocation density. Additionally, thicker coatings typically contain higher porosity and microcrack density, which further increases peak broadening. Therefore, the progressive increase in FWHM observed in thicker coatings explains why the calculated dislocation density increases with coating thickness, which is usually expected at thicker (or bulk) samples.

Copper radiation was used in the measurements, hence the wavelength (λ) was taken as 0.15406 nm, and the shape factor (k) was assumed as 0.94 due to the cubic crystal system. It should be noted that FWHM is influenced not only by dislocation density but also by crystallite size and microstrain.

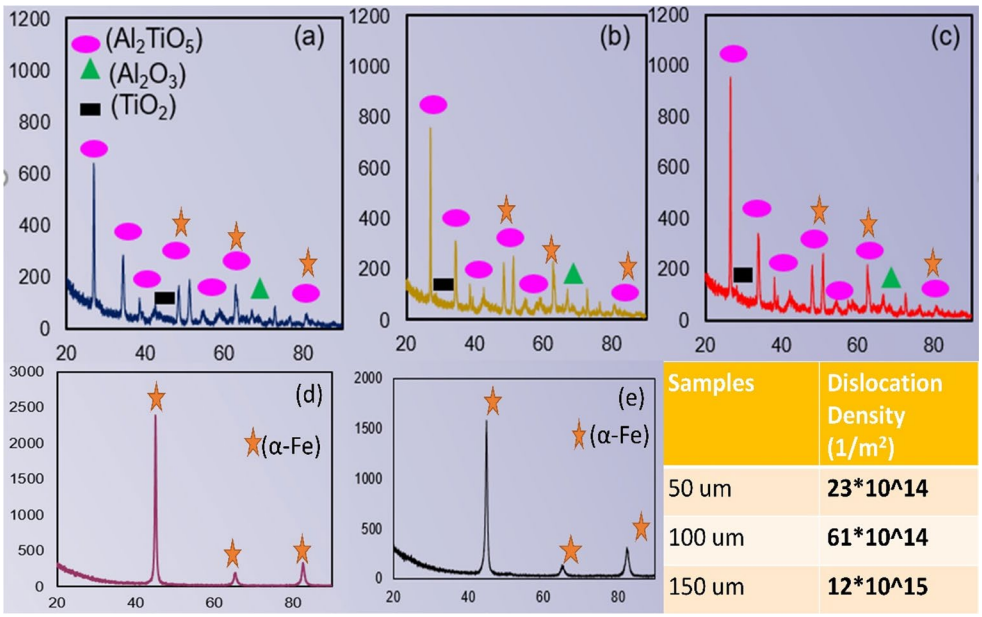
Williamson–Hall equation;

$\beta*\cos\theta = k*\lambda/D + \varepsilon(4\sin\theta)$ (1).

$\delta = 1/Dp2$ (1/m2) (2).

where β; FWHM of a diffraction peak (radyan), D; crystallite size. ε = lattice strain.

Figure 6 presents the surface microstructures of the samples after a 24-hour salt spray test. To evaluate the corrosion resistance of the coating, salt spray testing was conducted. In the present study, the 24-h duration was selected intentionally as a screening test to compare the relative corrosion resistance of the coatings prepared under different process parameters. This exposure time is commonly used in preliminary evaluations of ceramic-based thermal spray coatings. Longer duration tests (e.g., 72–168 h) were considered; however, the primary objective of this work was to understand early-stage corrosion mechanisms, pore sealing behavior, and the influence of coating thickness. Extending exposure beyond 24 h would introduce secondary degradation mechanisms that may obscure the comparative analysis between coatings. Figure 6 (a) shows the corrosion-induced surface of the untreated base material, while Fig. 6 (b) displays the surface of the heat-treated sample. Elemental analysis revealed the presence of Fe–O compounds at the crack tips and Na–Cl species within the crack zones. Figure 6(b)



Samples	Dislocation Density (1/m²)
50 um	23*10^14
100 um	61*10^14
150 um	12*10^15

Fig. 5 XRD graphs and dislocation density graphs of the samples. (**a**) 50 µm coating, (**b**) 100 µm coating, (**c**) 150 µm coating, (**d**) main materials (**e**) heat treatment materials

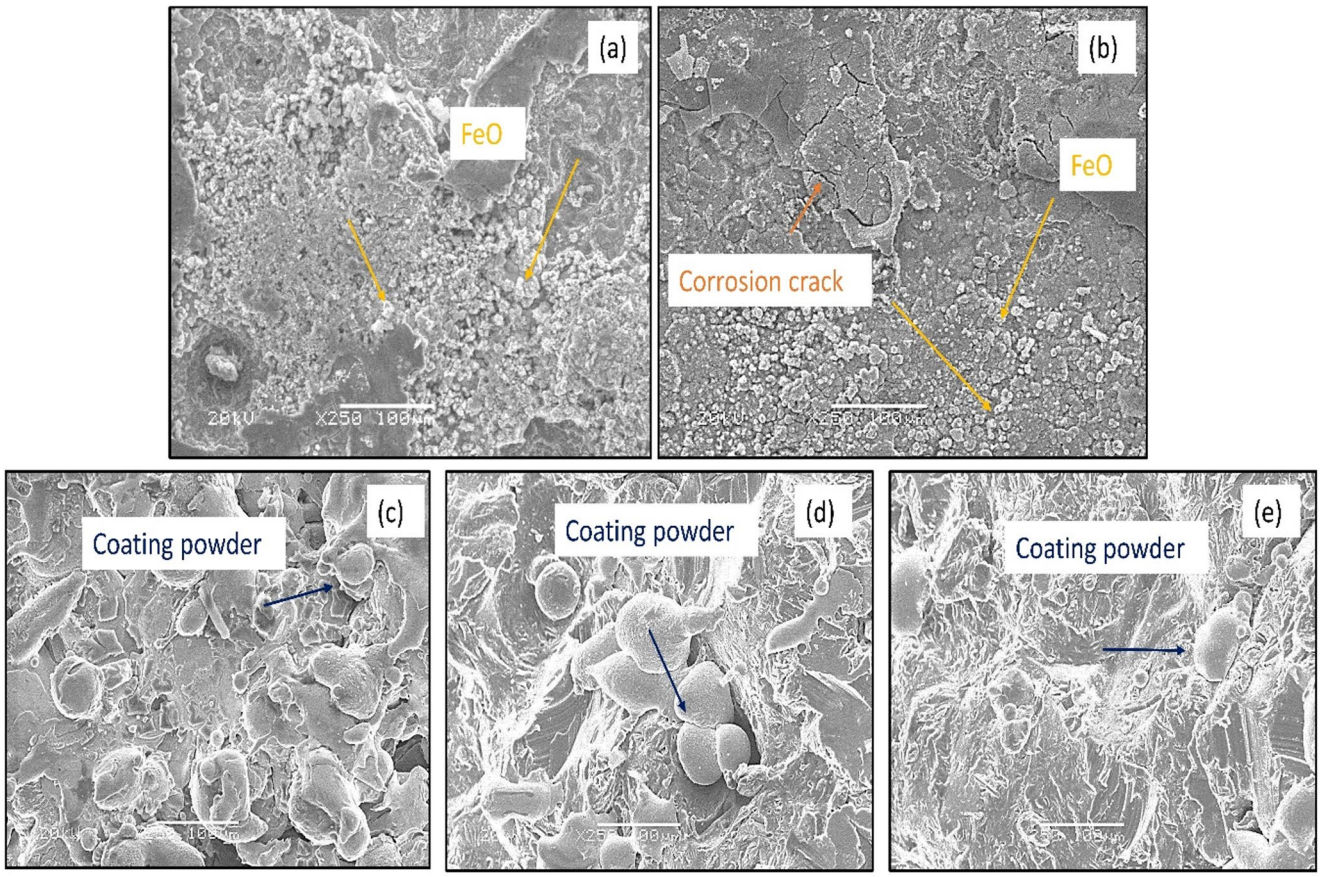


Fig. 6 Surface microstructures of samples after corrosion (**a**) main materials, (**b**) heat treatment, (**c**) 50 µm coating, (**d**) 100 µm coating, (**e**) 150 µm coating

shows that the formation of the tempered martensite structure after heat treatment also leads to the formation of corrosion cracks. This is because martensite behaves more anodic than austenite. In this case, a galvanic cell forms within the structure, and corrosion cracks become more pronounced. At the same time, the high internal stresses generated during the martensitic transformation created localized areas susceptible to corrosion [31]. Increased residual tensile stresses associated with martensitic transformation can adversely affect corrosion and oxidation rates, with inhomogeneous carbide distribution favoring microgalvanic activity and heterogeneous hard and brittle regions localizing corrosion attack [32]. Oxidized regions and discoloration were also observed in the corroded areas. Figures 6(c-d–e) show SEM images of the coated samples after corrosion testing, where no significant corrosion-induced cracks were observed. However, even if the coating itself remains unaffected during the salt spray test, a porous coating structure can allow chloride ions to penetrate beneath the coating and initiate corrosion in the underlying substrate. Therefore, low porosity in the coating is advantageous in improving corrosion resistance [33, 34].

4 Conclusions

In this study, flame-sprayed Al_2O_3–TiO_2 ceramic coatings were successfully applied to boron-alloyed microalloyed steel substrates, resulting in significant enhancements in surface performance. The findings obtained are as follows;

- SEM images showed good mechanical interlocking at the coating-substrate interface of all coatings made at 50 µm, 100 µm and 150 µm.
- The decrease in the density of the coated samples was due to both the porosity formed during the coating process and the inherently lower density of ceramic-based coating powders compared to steel.
- The 150 µm coated material with the lowest Wear Coefficient value shows that it is the material with the best wear resistance.
- Due to the tempered martensite structure, the hardness of the heat-treated material was measured as 580 HV1 and the hardness of the coated materials was measured as 720 HV1 on average.

- XRD analysis showed that as the coating thickness increased, the intensity of Al_2O_3 and TiO_2 peaks also increased. Dislocation density calculations were made between the coated materials. The highest dislocation density of the 150 µm coated sample was calculated as $12*10^{15}$.
- It was observed that corrosion cracks occurred in heat-treated samples due to martensite formation, while there were no signs of corrosion in coated samples.

Acknowledgements This study was supported by Gazi University Scientific Research Projects with project number FUİ-2025-10458.

Author Contribution G. Altuntas: Writing - original draft, Formal analysis, Methodology, Investigation.
F. Altun: Writing -original draft, Investigation.
(A) Bayar: Writing -original draft, Investigation.
R. Asmatulu: Writing - review & editing, Investigation.
(B) Bostan: Supervision, Resources, Writing - review & editing.

Funding Open access funding provided by the Scientific and Technological Research Council of Türkiye (TÜBİTAK).

Data availability The data that support the findings of this study are available from the corresponding author upon.
reasonable request.

Declarations

Conflict of interest The authors report no potential conflict of interest.

Open Access This article is licensed under a Creative Commons Attribution 4.0 International License, which permits use, sharing, adaptation, distribution and reproduction in any medium or format, as long as you give appropriate credit to the original author(s) and the source, provide a link to the Creative Commons licence, and indicate if changes were made. The images or other third party material in this article are included in the article's Creative Commons licence, unless indicated otherwise in a credit line to the material. If material is not included in the article's Creative Commons licence and your intended use is not permitted by statutory regulation or exceeds the permitted use, you will need to obtain permission directly from the copyright holder. To view a copy of this licence, visit http://creativecommons.org/licenses/by/4.0/.

References

1. M. Merklein, M. Wieland, M. Lechner, S. Bruschi, A. Ghiotti, Hot stamping of boron steel sheets with tailored properties: A review. J. Mater. Process. Technol. **228**, 11–24 (2016)
2. G.F. Melloy, P.R. Summon, P.P. Podgursky, Optimizing the boron effect. Metall. Trans. **4**(10), 2279–2289 (1973)
3. M. Vrolijk, D. Lorenz, H. Porzner, M. Holecek, Supporting lightweight design: virtual modeling of hot stamping with tailored properties and warm and hot formed aluminium. Procedia Eng. **183**, 336–342 (2017)
4. J. Lechler, T. Stöhr, A. Kuppert, M. Merklein, (2010, May). Basic investigations on hot stamping of tailor welded blanks regarding the manufacturing of lightweight components with functionally optimized mechanical properties. In Proc. NAMRC (pp. 593–600)
5. H. Li, L. He, G. Zhao, L. Zhang, Constitutive relationships of hot stamping boron steel B1500HS based on the modified Arrhenius and Johnson–Cook model. Mater. Sci. Engineering: A **580**, 330–348 (2013)
6. Y.P. Jeon, H.Y. Seo, J.D. Kim, C.G. Kang, Experimental analysis of coating layer behavior of Al–Si-coated boron steel in a hot bending process for IT applications. Int. J. Adv. Manuf. Technol. **67**(5), 1693–1700 (2013)
7. Z.X. Gui, W.K. Liang, Y. Liu, Y.S. Zhang, Thermo-mechanical behavior of the Al–Si alloy coated hot stamping boron steel. Mater. Design. **60**, 26–33 (2014)
8. Y. Zhang, B.A. Pint, G.W. Garner, K.M. Cooley, J.A. Haynes, Effect of cycle length on the oxidation performance of iron aluminide coatings. Surf. Coat. Technol. **188**, 35–40 (2004)
9. W.J. Cheng, C.J. Wang, Microstructural evolution of intermetallic layer in hot-dipped aluminide mild steel with silicon addition. Surf. Coat. Technol. **205**(19), 4726–4731 (2011)
10. M. Windmann, A. Röttger, W. Theisen, Phase formation at the interface between a boron alloyed steel substrate and an Al-rich coating. Surf. Coat. Technol. **226**, 130–139 (2013)
11. S. Amin, H. Panchal, A review on thermal spray coating processes. transfer. **2**(4), 556–563 (2016)
12. R. González, M. Cadenas, R. Fernández, J.L. Cortizo, E. Rodríguez, Wear behaviour of flame sprayed NiCrBSi coating remelted by flame or by laser. Wear. **262**(3–4), 301–307 (2007)
13. R.M. Trommer, C.P. Bergmann, *Flame spray technology* (Topics in Mining, Metallurgy and Materials Engineering, 2015)
14. L.M. Berger, Application of hardmetals as thermal spray coatings. Int. J. Refract. Met. Hard Mater. **49**, 350–364 (2015)
15. M. Naderi, M. Ketabchi, M. Abbasi, W. Bleck, Analysis of microstructure and mechanical properties of different boron and non-boron alloyed steels after being hot stamped. Procedia Eng. **10**, 460–465 (2011)
16. M. El-Shennawy, A.I. Farahat, M.I. Masoud, A.I. Abdel–Aziz, Heat treatment effect on micro–alloyed low carbon steel with different Boron content. Int. J. Mech. Eng. (IJME). **5**(4), 9–20 (2016)
17. H. Güler, R. Ertan, R. Özcan, Effect of heat treatment on the microstructure and mechanical properties of 30MnB5 boron steel. Mater. Technol. **48**(48), 971–976 (2014)
18. G. Altuntaş, Ö.F. Kaplan, B. Bostan, Investigation of the Effect of Tempering and Cryogenic Treatment on Mechanical Properties of Boron Steels. Gazi Univ. J. Sci. Part. C: Des. Technol. **11**(2), 300–308 (2023)
19. A. Bardelcik, M.J. Worswick, S. Winkler, M.A. Wells, A strain rate sensitive constitutive model for quenched boron steel with tailored properties. Int. J. Impact Eng. **50**, 49–62 (2012)
20. P. Leisner, M.E. Benzon, Porosity measurements on coatings. Trans. IMF. **75**(2), 88–92 (1997)
21. W.D. Callister, D.G. Rethwisch, *Fundamentals of materials science and engineering*, vol. 471660817 (Wiley, London, 2000)
22. C.J. Ridgway, P.A. Gane, Bulk density measurement and coating porosity calculation for coated paper samples. Nord. Pulp Pap. Res. J. **18**(1), 24–31 (2003)
23. J. Karthikeyan, M.M. Mayuram, Ceramic coating technology. Sadhana. **13**(1), 139–156 (1988)
24. Q. Cen, H. Fu, A study of heat treatment of high-boron high-speed steel roll. Materialwiss. Werkstofftech. **44**(7), 612–617 (2013)
25. R.A. Grange, C.R. Hribal, L.F. Porter, Hardness of tempered martensite in carbon and low-alloy steels. Metall. Trans. A **8**(11), 1775–1785 (1977)
26. M. Çivici, M. Özer, G. Altuntaş, T. Yilmaz, A.R. Shelar, O. Altuntaş, A. Özer, Advanced heat treatment strategies for

optimizing microstructure and mechanical integrity of AISI O2 tool steel. Ironmak. Steelmaking. **52**(9), 1232–1242 (2025)
27. O. Altuntaş, Crystallographic analysis of a new heat treatment strategy for improving the mechanical properties of powder metallurgical steel. Can. Metall. Q. **63**(4), 1061–1069 (2024)
28. K.A. Habib, J.J. Saura, C. Ferrer, M.S. Damra, E. Giménez, L. Cabedo, Comparison of flame sprayed Al2O3/TiO2 coatings: Their microstructure, mechanical properties and tribology behavior. Surf. Coat. Technol. **201**(3–4), 1436–1443 (2006)
29. A. Arsenlis, D.M. Parks, Modeling the evolution of crystallographic dislocation density in crystal plasticity. J. Mech. Phys. Solids. **50**(9), 1979–2009 (2002)
30. B. Himabindu, N.L. Devi, B.R. Kanth, (2021). Microstructural parameters from X-ray peak profile analysis by Williamson-Hall models; A review. Materials Today: Proceedings, 47, 4891–4896
31. L. Wang, C.F. Dong, C. Man, Y.B. Hu, Q. Yu, X.G. Li, Effect of microstructure on corrosion behavior of high strength martensite steel—A literature review. Int. J. Min. Metall. Mater. **28**(5), 754–773 (2021)
32. D. Dwivedi, K. Lepková, T. Becker, Carbon steel corrosion: a review of key surface properties and characterization methods. RSC Adv. **7**(8), 4580–4610 (2017)
33. A.S. Katarkar, B. Majumder, A.D. Pingale, S.U. Belgamwar, S. Bhaumik, (2021). A review on the effects of porous coating surfaces on boiling heat transfer. Materials Today: Proceedings, 44, 362–367
34. S. Deshpande, A. Kulkarni, S. Sampath, H. Herman, Application of image analysis for characterization of porosity in thermal spray coatings and correlation with small angle neutron scattering. Surf. Coat. Technol. **187**(1), 6–16 (2004)

Publisher's note Springer Nature remains neutral with regard to jurisdictional claims in published maps and institutional affiliations.